

# 1 Calculation of pressure- and migration-constrained dynamic CO<sub>2</sub> storage 2 capacity of the North Sea Forties and Nelson dome structures

3 Masoud Babaei<sup>1\*</sup>, Rajesh Govindan<sup>2</sup>, Anna Korre<sup>2</sup>, Ji-Quan Shi<sup>2</sup>, Sevket Durucan<sup>2</sup> and Martyn  
4 Quinn<sup>3</sup>

5 <sup>1</sup>School of Chemical Engineering and Analytical Science, University of Manchester, Manchester M13  
6 9PL, United Kingdom

7 <sup>2</sup>Department of Earth Science and Engineering, Royal School of Mines, Imperial College London,  
8 London SW7 2BP, United Kingdom

9 <sup>3</sup>British Geological Survey, The Lyell Centre, Edinburgh EH14 4AP, United Kingdom

## 10 Abstract

11 This paper presents a numerical simulation study of CO<sub>2</sub> injection into the Forties and Nelson dome  
12 structures in the North Sea. The study assumes that these structures are fully depleted of their  
13 remaining hydrocarbon and brine has replaced their pore space, and therefore the structures can be  
14 treated as saline aquifers. Under this assumption, the objective is to calculate the dynamic CO<sub>2</sub>  
15 storage capacity of the Forties and Nelson structures and design an injection scenario to enhance  
16 storage utilisation. In doing so, first, a detailed geological model of the dome structures and their  
17 surrounding aquifer is developed to represent the lithological facies associations and attribute them  
18 with petrophysical properties. The geological model is calibrated in terms of the surrounding aquifer  
19 support using the hydrocarbon production data. The dynamic storage capacity is subsequently  
20 estimated by numerical simulation of the two-phase (brine and CO<sub>2</sub>) process. Key performance  
21 indicators (KPIs), such as the pressure build-up and regional mass fraction of CO<sub>2</sub>, are used to  
22 constrain the injection scenarios that consequently result in the best capacity utilisation of the  
23 storage structures. In our model of fully brine saturated dome structures, based on specific  
24 constraints, namely <0.1% of the total gaseous CO<sub>2</sub> outside the dome into an upper pressure unit  
25 and 66% of the initial hydrostatic pressure as the allowable increase in the bottom-hole pressure, we  
26 obtained a dynamic capacity of 121 million tonnes for the Forties structure and 24 million tonnes for  
27 the Nelson structure. These values are subject to change when a three phase model of residual oil,  
28 gas and water is considered in simulations.

## 29 1. Introduction

30 The storage of carbon dioxide in depleted or mature oil or natural gas reservoirs has obvious  
31 advantages over storage in pristine aquifers where we have a limited and uncertain knowledge of  
32 the geological environment, namely their trapping potential or storage capacity. Porous rock  
33 formations that are proven traps have retained hydrocarbons for millions of years, and are potential  
34 candidates for CO<sub>2</sub> storage (IPCC, 2005). Moreover, this option may even be economically  
35 sustainable as it can enhance oil or gas recovery (EOR/EGR). Hence, CO<sub>2</sub> injection operations in  
36 mature reservoirs are the ones most likely to be implemented first, because of the additional  
37 economic benefit that will help offset the cost of CO<sub>2</sub> storage (Holt et al., 1995; Stevens et al., 2000).

38 Two reservoirs that have been considered for potential CO<sub>2</sub> storage through EOR in the UK Sector of  
39 the Central North Sea are the Forties and Nelson oilfields (Espie, 2001; Cawley et al., 2005; SCCS,  
40 2009) which feature high-quality channel sands. Previously, Ketzer et al. (2005) evaluated the long  
41 term CO<sub>2</sub> leakage risk from the Forties reservoir assuming that it was filled with supercritical CO<sub>2</sub>.

---

\* Corresponding author: The University of Manchester, School of Chemical Engineering and Analytical Science,  
[masoud.babaei@manchester.ac.uk](mailto:masoud.babaei@manchester.ac.uk), t: +44 (0)161 306 4554

42 They reported that the CO<sub>2</sub> plume would travel only a small distance in the overburden during the  
43 post-injection period. Cawley et al. (2005) reported that after the injection of CO<sub>2</sub> into the depleted  
44 Forties Field, CO<sub>2</sub> would not exceed the capillary entry pressure of the overburden. They also  
45 reported that, due to the absence of major faults, the thickness of the reservoir and very low  
46 permeability of its overburden, the Forties Field is an ideal structure for CO<sub>2</sub> storage. In none of  
47 these studies, however, has a storage capacity estimation of the Forties Field and the neighbouring  
48 Nelson Field been presented, where the pressure communication and fluid migration between the  
49 two structures that form a part of Forties Sandstone Member are considered in storage performance  
50 assessments.

51 Against this backdrop, we conduct a study in this paper, relying on a large and complex geological  
52 model of the two structures in communication with their surrounding aquifer, to estimate the  
53 dynamic capacity estimates of the Forties and Nelson fields, assuming that the structures could be  
54 treated as saline aquifers. This assumption, which may be unrealistic, is made because our three-  
55 phase simulations of the CO<sub>2</sub> injection into the geological model had convergence issues and  
56 required prohibitive computational power. Consequently, the results of this work may serve as crude  
57 and approximate estimates for the static and dynamic storage capacities of the Forties and Nelson  
58 structures neglecting the three-phase complexities and differences with two-phase systems, and  
59 provide dynamic capacity estimates of the storage in comparison to the reported static estimates for  
60 the same structures. Examples in the literature of presented estimates are SCCS (2009) that reported  
61 138 million tonnes CO<sub>2</sub> capacity for the Forties oilfield by the CO<sub>2</sub>-EOR process. Assuming a range of  
62 0.2%–2% storage efficiency, they reported storage capacities of 886–8,856 million tonnes CO<sub>2</sub>.  
63 Elsewhere, Espie (2001) reported that at least 75 million tonnes of CO<sub>2</sub> could be stored underground  
64 as a result of EOR in the Forties Field, with further potential if storage was continued for its own sake  
65 after EOR.

66 In this paper we will use the numerical simulation as the most sophisticated method of estimating  
67 dynamic CO<sub>2</sub>-storage capacity. Examples of dynamic methods are decline-curve analysis (Frailey,  
68 2009), material balance (Mathias *et al.*, 2009; Zhou *et al.*, 2008), and reservoir simulation-based  
69 approaches (e.g., Doughty and Pruess, 2004; Kumar *et al.* 2004; Ennis-King and Paterson, 2005; Ozah  
70 *et al.*, 2005; Flett *et al.*, 2007; Yamamoto *et al.*, 2009 and Liao *et al.*, 2014). A full review of the  
71 dynamic storage capacity estimation in comparison with static methods is presented in Bachu *et al.*  
72 (2015). The numerical methods have the advantage of being able to take into account the  
73 heterogeneity of the storage site and trapping of CO<sub>2</sub> by various storage mechanisms that are  
74 involved in the storage process. They also account for the physical processes which are important for  
75 CO<sub>2</sub> storage, such as the build-up of pressure in the near-well region and throughout the storage  
76 site, and migration of CO<sub>2</sub> by advection and buoyancy. Birkholzer et al. (2015) thoroughly surveyed  
77 pressure build-up issue and its direct implications on utilizing the storage capacity.

78 We will use the pressure build-up and migration that may critically affect the storage capacity of  
79 aquifer structures to define key performance indicators (KPI's) to assess the injection process as well  
80 as to define constrained injection strategies. We will use a novel injectivity-index-weighted dynamic  
81 apportioning of rate between a series of fixed injection wells. Injectivity and its dynamic variations  
82 are assumed as important factors to be considered in the optimal design of storage capacity  
83 utilization (van der Meer and Egberts, 2008; Burton et al., 2008; van der Meer and Yavuz, 2009). The  
84 methodology proposed here takes into account effects of the geological model properties on the  
85 wells' injectivities and the inflow performances, and dynamic variations of injectivities. Migration  
86 and pressure build-up control measures are also simultaneously applied to produce a set of  
87 dynamically varying injection rates so that an optimal injection scenario can be designed.

88 *Outline:* In the sections that follow, first we describe the geological model of the dome structures in  
89 Section 2 (with extra information about the geological settings and model construction in the

90 Appendix). Next in Section 3, a calibration exercise is presented in which the aquifer support of the  
91 study area is adjusted using the pressure behaviour of the hydrocarbon reservoirs. In Section 4, the  
92 KPI's are defined and the methodology to extract injection rates based on the dynamically varying  
93 injectivity of the injection wells is presented. The results are given in Section 5 and conclusions and  
94 future work in Section 6.

## 95 2. Study area and geological model

96 The study area is located on the Forties-Montrose High in the UK Central North Sea (Figure 1a). The  
97 3D model has been built around an area that includes the Forties and Nelson hydrocarbon fields that  
98 are four-way dip closed structures containing sandstone reservoirs capped by a thick mudstone-  
99 dominated seal. There are four main production platforms, evenly spaced over the area of the  
100 Forties field: Forties Alpha (FA), Bravo (FB), Charlie (FC) and Delta (FD), and an auxiliary platform  
101 Forties Echo (FE) (Figure 1b). There is only one platform for the Nelson reservoir which is referred to  
102 as N in DECC's database for production wells in the North Sea (DECC, 2007). The depth map of the  
103 top surface of the 3D model is shown in Figure 1c.

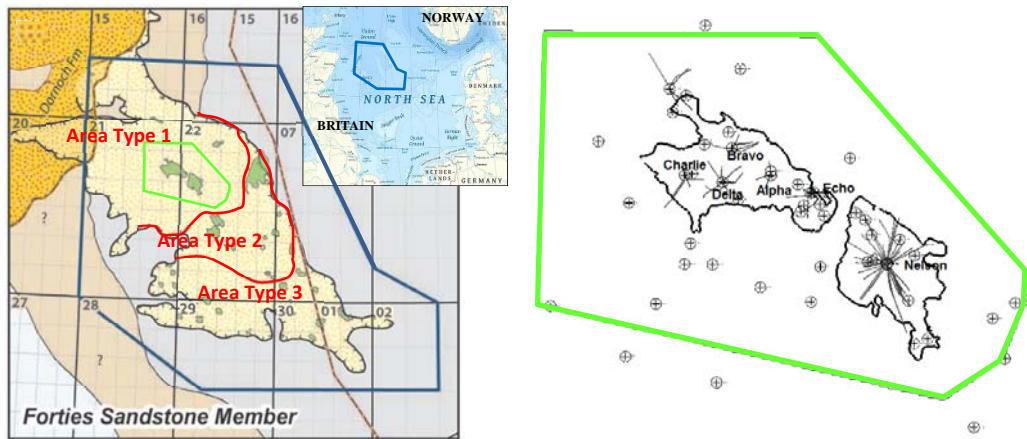
104 The hydrocarbon reservoirs of the Forties and Nelson fields are submarine fan deposits contained in  
105 the Upper Paleocene/ Lower Eocene Sele Formation and overlain by Lower Eocene shales (Hughes *et*  
106 *al.*, 1990; Whyatt *et al.*, 1992). The reservoirs are located in the proximal inner (interbedded  
107 sand/shale) to middle (mainly massive sand) fan region (Hughes *et al.*, 1990) and are mostly  
108 channelised and characterised by high net to gross ratios, good porosities and high permeabilities  
109 (Hempton *et al.*, 2005). Detailed geological modelling of the Forties and Nelson hydrocarbon fields in  
110 the UK sector of the North Sea has been reported by Kulpecz and van Geuns (1990) and Kunka *et al.*  
111 (2003).

112 The geological model developed in this study broadly captures and represents the heterogeneities  
113 present within what is a very complex submarine fan environment. The fan system within the two  
114 fields comprises the main hydrocarbon producing fairways: large amalgamated stacked channel  
115 systems of the Late Paleocene/ Early Eocene Forties Sandstone Member within four-way dip-closed  
116 anticlinal structures. Along with the channels are the associated channel margins and interchannel  
117 areas. The varying relative dominance and position of the different parts of the submarine fan  
118 system through time resulted in a high degree of lateral and vertical variation. This is represented in  
119 the lithologies found in the system and their associated petrophysical parameters.

120 The structural zonation schemes in each of the fields have been unified and extended out with the  
121 field areas (Table 1). The geological model consists of 5 reservoir Zones (E, F, H, J and K), capped by a  
122 seal (Zones M and L). The reservoirs overlie a field-wide discontinuity between Zones E and D, so  
123 that Zone D is mostly (for Forties) or entirely (for Nelson) under the water-oil-contact. The geological  
124 model contains a field-wide permeability barrier between Zones H and J. This barrier is also referred  
125 to as Charlie Shale that produces a notable pressure discontinuity over the west and centre of the  
126 Forties field but is thin and discontinuous in the east and south-east of the field. In the east over the  
127 Nelson Field the barrier forms part of the top seal, therefore the caprock is thicker for Nelson than  
128 Forties. Consequently, most of the Forties Field and a small part of the Nelson Field are divided into  
129 two pressure units: Zones J and K (upper pressure unit), and Zones E, F and H (lower pressure unit).  
130 Other partially extensive barriers (notably between Zones E and F, and between Zones F and H) are  
131 modelled by vertical permeability multipliers. As Zone D is mostly or entirely below the water-oil  
132 contact lines of both reservoirs, and Zones M and L form a seal for Forties, only Zones K, J, H, E and F  
133 are considered in the study since they include the reservoir units.

134

135

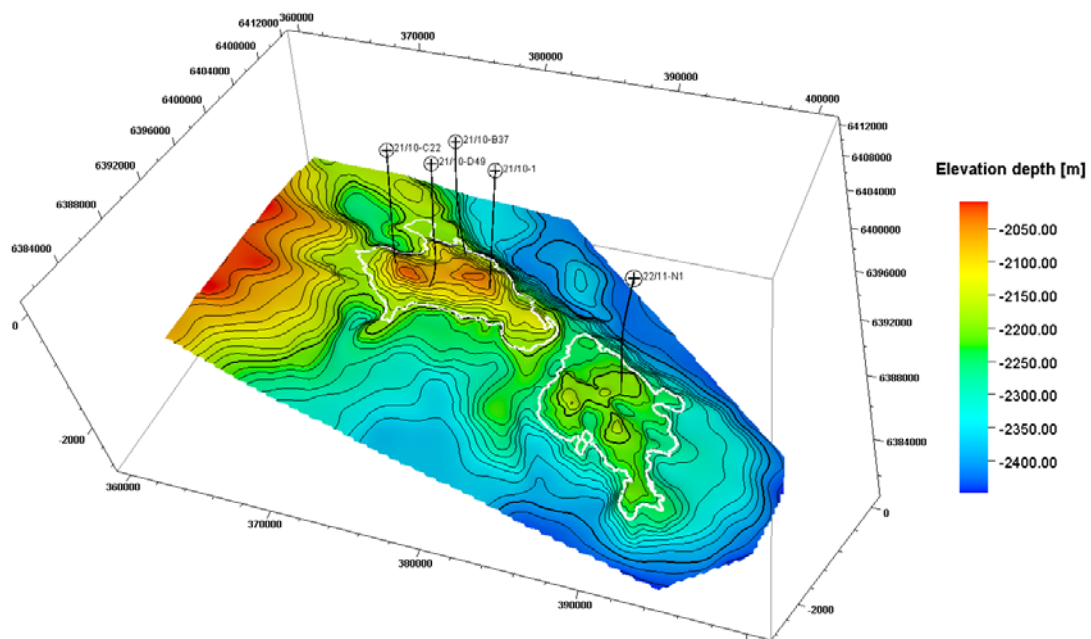


136

137

(a)

(b)



138

139

(c)

140 **Figure 1.** (a) Central North Sea region showing the distribution of the Forties Sandstone Member, known  
 141 hydrocarbon accumulations in the member (Robertson et al., 2013), and three Area Types as  
 142 defined in the Appendix. The study area is shown by a neon green template. (b) The location of the  
 143 production platforms in Forties: Forties Alpha (FA), Forties Bravo (FB), Forties Charlie (FC), Forties  
 144 Delta (FD) and auxiliary Forties Echo (FE), and single platform in Nelson. The wells that are scattered  
 145 across the region have been used for water injection. (c) The elevation map of the top surface of the  
 146 study area and the wells used for injection in this study namely 21/10-1 at FA, 21/10-B37 at FB,  
 147 21/10-C22 at FC, 21/10-D49 at FD, and 21/11-N1 at N. The vertical direction is exaggerated by a  
 148 factor of 10.

149

150 **Table 1.** Unification of geological model zonation in Forties by Wills (1991) and Nelson by Kunka *et*  
 151 *al.* (2003)

<b>Our Model</b>	<b>FORTIES Model of Wills (1991)</b>	<b>NELSON Model of Kunka (2003)</b>	<b>Facies</b>	<b>Average Thickness (meter)</b>
Zone M (caprock of Sele Formation)	Unit M		mudstone	37
Zone L (caprock)	Unit L	Partially present and very thin over Nelson	mudstone	8
Zone K (upper pressure unit)	Unit K	Partially present and very thin over Nelson	thick bedded sandstone and interbedded sandstone and mudstone	14
Zone J (upper pressure unit)	Unit J			44
Field-wide pressure discontinuity (Charlie Shale)				15
Zone H (lower pressure unit)	Unit H	Zone 5	thick bedded sandstone, and interbedded sandstone and mudstone	22
Zone F (lower pressure unit)	Unit F	Zone 4		39
Zone E (lower pressure unit)	Unit E	Zone 3		40
Field-wide pressure discontinuity				25
Zone D (below oil-water contact)	Unit D	Zones 1 & 2	succession of thin bioturbated sandstones and mud-rich conglomerate	123

152 The positions of the channels in each zone and the extent of the Forties and Nelson fields that lay  
 153 inside each of these zones are illustrated in Figure 2. The extent of storage domes is determined  
 154 from topography and the original oil-water contact of the reservoir.

155 Figure 2 also shows the regionalisation of the different zones of the model based on whether they  
 156 are located inside or outside the structure domes. In order to set this up, we used the horizon  
 157 surfaces of the different zones in the model and the initial water-oil contact planes of the Forties and  
 158 Nelson reservoirs, located at 2217 m and 2270 m depth respectively.

159

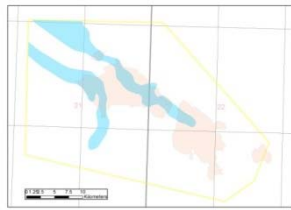
160

161

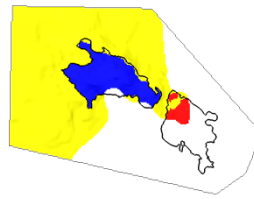
162

163

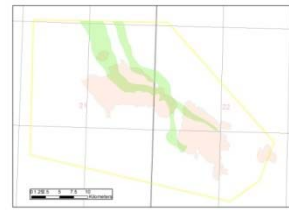
164



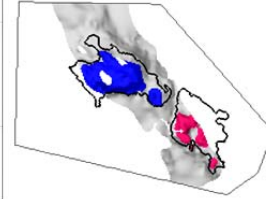
(a)



(b)



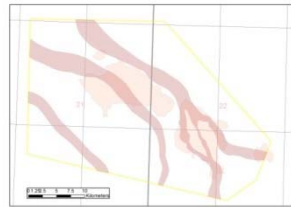
(c)



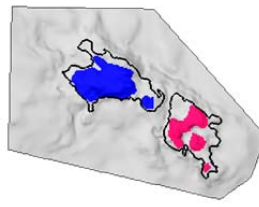
(d)

165

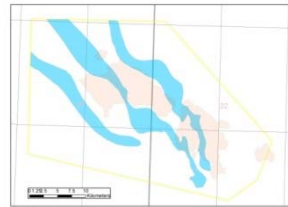
166



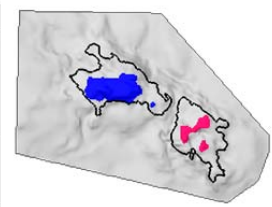
(e)



(f)



(g)



(h)

167

168

169

170

171

172

173

174

**Figure 2.** (a) The position of channels in **Zones J and K**, (b) regional divisions of Zone J and K, (c) the position of channels in **Zone H** beneath Charlie Shale, (d) regional divisions of Zone H, (e) the position of channels in **Zone F**, (f) regional divisions of Zone F, (g) the position of channels in **Zone E**, (h) regional divisions of Zone E. In (b), (d), (f) and (h) yellow represents part of the Zones J and K that lies outside the Forties and Nelson domes, grey represents part of the Zones E, F and H that lies outside the Forties and Nelson domes, blue the parts that lie within the Forties dome and red the parts that lie within the Nelson dome.

175

176

177

178

179

The attribution of the geological model with petrophysical properties, namely porosity, permeability and net-to-gross (NTG) ratio, was carried out using Gaussian random functions. The ranges of values used, including their mean values, are summarised in Table 2 for the different geological facies associations. Some of these values are based on generalisations from the literature such as Kunka *et al.* (2003) and Wills (1991), and in absence of data, average values were assumed by the authors.

180

181

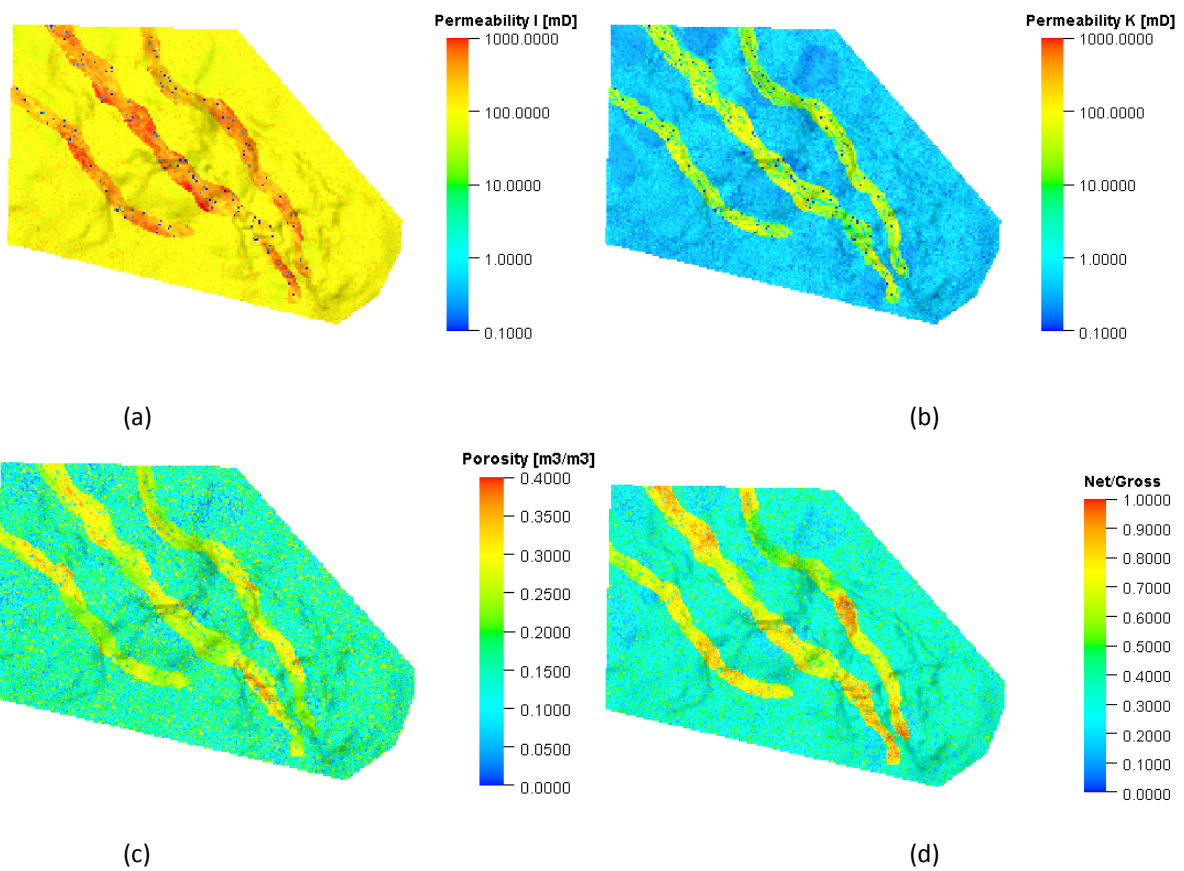
182

**Table 2.** Petrophysical properties for different facies types from Kunka *et al.* (2003) and Wills (1991) and well log analyses; values indicated as mean (minimum, maximum). For additional information about different facies mentioned in this table please refer to the Appendix.

Petrophysical property	Channel sands	Basal lags (low permeability)	Basal lags (high permeability)	Shale doggers	Interchannel (Slump debris and Mudstones)	Slump bodies
Porosity (%)	25 (21, 38)	25 (21, 38)	25 (21, 38)	< 12	24.6 (3, 32.9)	13 (3, 32.9)
Horizontal Permeability (mD)	376 (31, 1,610)	376 (31, 1,610)	376 (31, 1,610)	< 1	163 (0.01, 1,769)	50 (0.01, 1,769)
Vertical Permeability (Multiplier)	0.1	0.01	0.1	1	0.001-0.01	0.001-0.01
NTG	0.72 (0.21, 1)	0.72 (0.21, 1)	0.72 (0.21, 1)	0.21 (0.21, 1)	0.33 (0.11, 0.89)	0.11 (0.11, 0.89)

183

184 A realisation was generated based on the above-mentioned properties at a grid resolution of 100 m  
185  $\times$  100 m  $\times$  2 m. The profiles of horizontal and vertical permeability, porosity and net-to-gross ratio  
186 are shown in Figure 3. The same realisation with the specified resolution is used for flow modelling.



187  
188

189

190

191

192

**Figure 3.** (a) Horizontal permeability (millidarcy), (b) vertical permeability (millidarcy), (c) porosity, and (d) net-to-gross ratio for top of Zone E.

193

### 3. Simulation of hydrocarbon production for calibrating the model

In this section the aquifer model is calibrated using historical hydrocarbon production and water injection data from the DECC database (DECC, 2007), as well as the historical pressure data found in the literature. Some of the properties of the hydrocarbon and resident water derived from literature for the two oil fields are summarised in Table 3. The oil-gas and water-gas relative permeability curves are derived from Cawley *et al.* (2005) who studied an enhanced oil recovery using CO<sub>2</sub> at a segment of the Forties Field. It is assumed these curves are applicable for the fluids across the entire domain of the study area in this work.

**Table 3.** Reservoir fluid properties from Wills (1991), and Kunka *et al.* (2003).

	Forties	Nelson
<b>Hydrocarbon</b>		
Initial oil saturation [ $S_{oi}$ ]	≈0.85	≈0.80
Initial oil in place [ $V_{osi}$ ] (standard million m <sup>3</sup> or sm <sup>3</sup> )	690	125
Formation volume factor [ $B_o$ ] (reservoir m <sup>3</sup> /standard m <sup>3</sup> or rm <sup>3</sup> /sm <sup>3</sup> )	1.24–1.32	1.36
Initial oil in place (reservoir million m <sup>3</sup> ) [ $V_{oi} = V_{osi} \times B_o$ ]	≈883	170
Dome volume above water-oil contact (reservoir million m <sup>3</sup> ) [ $V_{oi}/S_{oi}$ ]	1,038	212
Recovery factor by 2013	0.62	0.58
<b>Formation water</b>		
Salinity (ppm of NaCl)	55,500	84,000
Resistivity (ohm m)	0.034	N/A
<b>Reservoir conditions</b>		
Temperature (°C)	96 at 2175	107 at 2255 m
Initial pressure (bar)	222 at 2175 m	229
Oil-water contact	2217 m	2270 m

In addition to the data above, we assume formation brine has a coefficient of isothermal compressibility of  $3.5 \times 10^{-5} \text{bar}^{-1}$  and rock has a coefficient of isothermal compressibility of  $4.5 \times 10^{-5} \text{bar}^{-1}$ .

An objective of the model calibration is to determine the pore volume multiplier (PVM) that will be used in the simulations to establish the boundary conditions accounting for the pressure support from the surrounding aquifer system. PVM applied on the boundary grid blocks effectively enlarges the domain, which in turn has a direct effect on the pressure behaviour. Obviously, the larger the value of the multiplier, the less the pressure depletion during production will be. In order to establish a reasonable value, the data for pressure decline at start of the production and the pressure build-up at start of the water injection are also used.

According to Brand *et al.* (1996) and Wills (1991), in the first 5 years after production started (by start of 1981), the pressure in the oil bearing sandstone layers of Forties declined by 55-70 bar below the original level. Brand *et al.* (1996) provided pressure depletion profiles in two sandstone regions of Forties (Zones E, F and H in the centre and east and Zones J and K in the west). Permeability restrictions exist between the sand bodies of the field (south-east Forties) that cause significant pressure differences between them (Brand *et al.*, 1996).

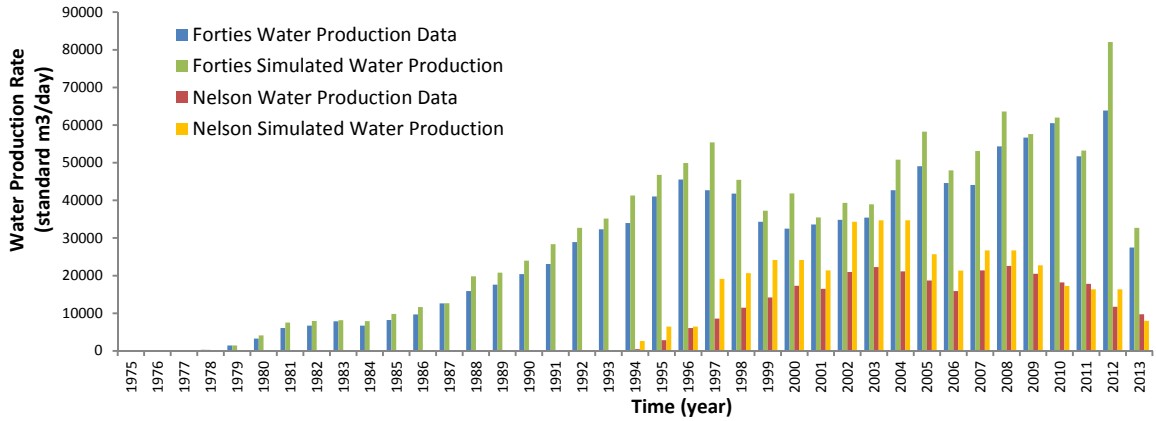
With the aquifer support having come into effect, coupled with the increasing water injection by 1994, the reservoir pressure rose back to around 14 bar below the original hydrostatic level. Moreover, Simpson and Paige (1991) report that the Forties reservoir pressure was maintained by basal aquifer influx initially, prior to the supplementation of peripheral seawater injection. For the Nelson Field, it is reported by Kunka *et al.* (2003) that by July 1997, 3 years after the production started, the pressure depletion was similar to Forties, around 55-70 bar below the initial level. Here,



225 it is assumed that the pressure drop would be compensated by a combination of the basal aquifer  
226 support and peripheral seawater injection over time.

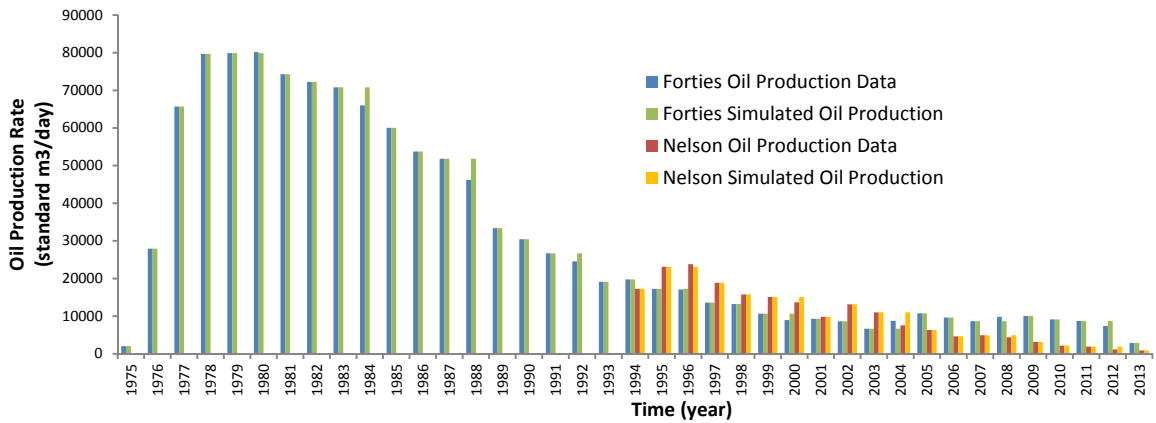
227 Based on the above information and assumptions, the PVM is determined by matching the  
228 simulated regional pressures with pressure behaviour of the Forties and Nelson oilfields. The target  
229 is a post-production average pressure decline of around 70 bar over the oilfield regions that can be  
230 compensated later on during the simulation. The multiplier of PVM = 20 that leads to a reasonable  
231 behaviour of the field pressure in the production stage is used for the CO<sub>2</sub> injection simulations. This  
232 multiplier applied on the boundary blocks increased the formation pore volume in the whole system  
233 from 8,552 million rm<sup>3</sup> to 42,548 million rm<sup>3</sup>.

234 The yearly cumulative oil and water production from Forties and Nelson are shown in Figure 4(a) and  
235 Figure 4(b). Except for the overestimations of water production at some stages, the graphs show a  
236 good agreement between the simulation results and the actual data. The average pressure for areas  
237 including Forties and Nelson are shown in Figure 4(c). A post-production pressure decline of up to 70  
238 bar is observed that was later compensated for by water injection and water influx from the  
239 boundaries. It is noted that the pressure profiles from literature and simulation do not accurately  
240 represent the true average pressures from the geological units; however, the trends are in  
241 reasonable agreement. Another reason for the observed discrepancy and delayed pressure recovery  
242 of our model against the existing data can be probably linked to the insufficiency of considering PVM  
243 as the only parameter for model calibration. A PVM > 20 would create pressure profiles with too  
244 small reduction during initial years, whereas a PVM < 20 result in pressure profiles with too large  
245 reduction during initial years and too little post-water-injection increase. In conclusion, based on a  
246 reasonable agreement between data and our model, the assumption will be made that the pressure  
247 has been restored to the initial hydrostatic level prior to CO<sub>2</sub> injection.



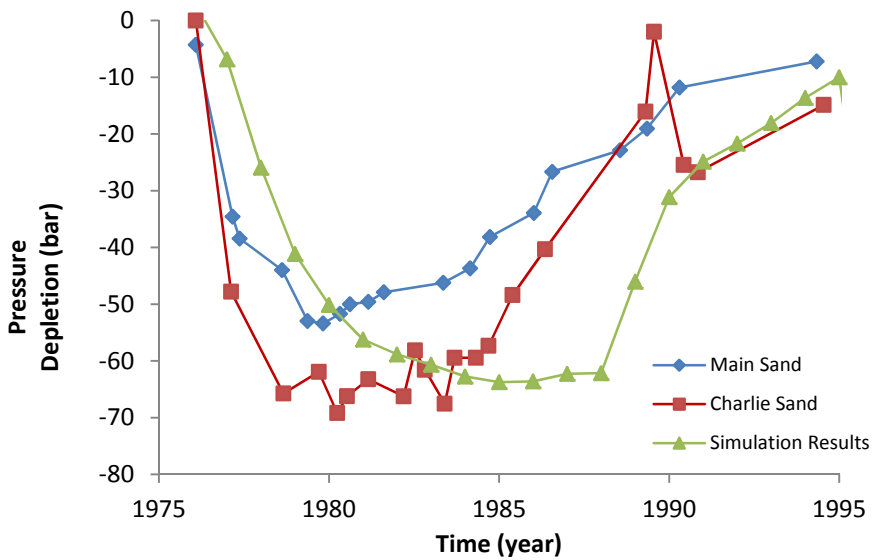
248  
249

(a)



250  
251  
252

(b)



253  
254

(c)

**Figure 4.** (a) The yearly oil production rates from the Forties and Nelson oilfields, (b) the yearly water production rates from the Forties and Nelson oilfields, simulation results compared to the actual data from DECC (2013). (c) The pressure depletion profiles from the hydrocarbon production simulation. Also shown are the field data for Charlie Sand (mostly coinciding with Zones J and K) and Main Sand (mostly coinciding with E, F and H) from Brand *et al.* (1996).

259

## 260 4. Dynamic capacity calculation

### 261 4.1 Definitions of the key performance indicators (KPIs)

262 To assess injection scenarios, a number of KPIs are defined and calculated throughout the injection  
263 and post-injection periods. These parameters are:

264 1) Well bottomhole pressure build-up ratio:

$$r_{p,W}^t = \frac{p_{bh,W}^t}{p_{h,i}^{t_0}} \quad (1)$$

265 where  $p_{bh,W}^t$  represents the well bottomhole pressure of a well  $W$  at a simulation time  $t$ ,  
266  $p_{h,i}^{t_0}$  represents the hydrostatic pressure at initial time  $t^0$  of the block  $i$  in the  $100 \text{ m} \times 100 \text{ m}$   
267  $\times 2 \text{ m}$  grid. Therefore  $r_{p,W}^t$  is the ratio of the well bottomhole pressure over the initial  
268 hydrostatic pressure of the perforated depth. This measure indicates the local pressure  
269 increase of the system due to  $\text{CO}_2$  injection and should be limited to some certain values  
270 according to the fracture pressure avoidance constraint.  
271

272 2) Mass fraction of  $\text{CO}_2$  in various regions of the domain:

$$x_{m,R}^t = \frac{m_{\text{CO}_2,R}^t}{m_{\text{CO}_2}^t} \quad (2)$$

273 where  $m_{\text{CO}_2,R}^t$  represents the mass of  $\text{CO}_2$  present in a region  $R$  at a simulation time  $t$  and  
274  $m_{\text{CO}_2}^t$  represents the total mass of  $\text{CO}_2$  injected into the system by simulation time  $t$ .  
275 Therefore  $x_{m,R}^t$  is the mass fraction of injected  $\text{CO}_2$  in region  $R$  at simulation time  $t$ .  
276 To help track the  $\text{CO}_2$  plume movement and spillage outside the storage dome, the model  
277 domain is divided into four control regions:

- 278 ▪ the Forties dome: *Region 1*
- 279 ▪ the Nelson dome: *Region 2*
- 280 ▪ areas lying outside the domes in Zones J and K (Forties upper pressure unit): *Region 3*
- 281 ▪ areas lying outside the domes in Zone E, F and H (Forties lower pressure unit): *Region 4*
- 282
- 283

284 We define:

$$x_{m,1}^t = \frac{m_{\text{gaseous CO}_2,R1}^t + m_{\text{dissolved CO}_2,R1}^t}{m_{\text{CO}_2}^t}$$

$$x_{m,2}^t = \frac{m_{\text{gaseous CO}_2,R2}^t + m_{\text{dissolved CO}_2,R2}^t}{m_{\text{CO}_2}^t}$$

$$x_{m,3}^t = \frac{m_{\text{gaseous CO}_2,R3}^t}{m_{\text{CO}_2}^t}$$

$$x_{m,4}^t = \frac{m_{\text{gaseous CO}_2,R4}^t}{m_{\text{CO}_2}^t} \quad (3)$$

288 where  $x_{m,1}^t$  and  $x_{m,2}^t$  indicate the level of containment of  $\text{CO}_2$  inside the Forties and Nelson  
289 structures, and  $x_{m,3}^t$  and  $x_{m,4}^t$  indicate the gaseous  $\text{CO}_2$  remained outside of the dome  
290 structures at time  $t$ . Only the gaseous portion of  $\text{CO}_2$  is considered in  $x_{m,3}^t$  and  $x_{m,4}^t$ , because  
291  
292

293 it is assumed that the dissolved CO<sub>2</sub> implies less risk of leakage to the surface from regions  
 294 outside the dome structures. Therefore  $x_{m,3}^t$  and  $x_{m,4}^t$  cannot be used for mass balance  
 295 calculations, and they are defined as such only for leakage potential. It should be noted that  
 296 Region 3 lies in Zones J and K (the part of Forties upper pressure unit shown in yellow in  
 297 Figure 2b), which is penetrated by a large number of abandoned wells. This, together with  
 298 the fact that Zone J is also in immediate contact with the caprock, makes this region prone  
 299 to risk of CO<sub>2</sub> leakage through abandoned wells and the caprock outside of the dome.  
 300 Therefore, reducing  $x_{m,3}^t$  must be one objective of the injection design.

301 3) Fraction of capacity utilised:

$$e_{V,R}^t = \frac{V_{CO_2,R}^t}{PV_R} \quad (4)$$

302 where  $V_{CO_2,R}^t$  represents the summation of gaseous and aqueous volumes of CO<sub>2</sub> at reservoir  
 303 conditions in a region  $R$  at a simulation time  $t$  and  $PV_R$  represents the pore volume of the  
 304 region  $R$  at reservoir conditions. Therefore  $e_{V,R}^t$  is the fraction of capacity of the region  $R$   
 305 utilised at simulation time  $t$ . Obviously, the larger this value is, the more efficient the  
 306 storage operation is. It should be noted that this metric should not be confused by  
 307 commonly used "storage efficiency" defined by van der Meer (1995) as "the ratio between  
 308 the maximum storage volume and the actual injected volume." Here this metric is calculated  
 309 in terms of the volume of CO<sub>2</sub> injected in the section of the reservoir formation that is inside  
 310 the perimeter of the reservoirs' boundaries rather than the whole aquifer volume and  
 311 therefore the values will be higher than the storage efficiency values because the  
 312 denominator is much smaller.  
 313

314 In our model,  $PV_R$  for Region 1 is 1,042 million  $rm^3$  (compared to 1,038 million  $rm^3$  in Table 3 for  
 315 Forties dome), for Region 2,  $PV_R$  is 219 million  $rm^3$  (compared to 212 million  $rm^3$  in Table 3 for  
 316 Nelson dome), for Region 3,  $PV_R$  is 4,435 million  $rm^3$  and for Region 4,  $PV_R$  is 36,852 million  $rm^3$ ,  
 317 note that PVM acts only on the pore volume of the boundary blocks of Regions 3 and 4. The  
 318 discrepancies between the pore volumes of our model and the actual reservoirs can be attributed to  
 319 the stratigraphical inaccuracies.

## 320 4.2 Definitions of constrained injection scenarios

321 For calculating the dynamic capacity of the Forties Field and at the same time utilising its storage  
 322 capacity optimally, four vertical injection wells were located on the main platforms in Forties and  
 323 one was placed on the Nelson Field platform. The injection pressure is constrained so as not exceed  
 324 0.9 multiplied by the fracture pressure of the injection depth:

$$p_{bh,W}^t \leq 0.9 \times p_{f,W} \frac{p_{f,W}=(g_f/g_h)p_{h,i}^{t_0}, \quad r_{p,W}^t=p_{bh,W}^t/p_{h,i}^{t_0}}{\rightarrow} r_{p,W}^t \leq 0.9 \times g_f/g_h \quad (5)$$

326 where  $p_{f,W}$  is the fracture pressure at perforation depth of well  $W$ ,  $g_f$  is the fracture gradient of the  
 327 system,  $g_h$  is the hydrostatic gradient of the system, and  $p_{h,i}^{t_0}$  is the initial hydrostatic pressure  
 328 (defined at the centre of the 100 m × 100 m × 2 m gridblock,  $i$ ) at a reference depth of top of Zone H  
 329 where bottomhole pressure of well  $W$  is also calculated. All the wells are assumed to be 0.3048  
 330 metres in diameter, the fracture gradient for the Forties Sandstone Member is assumed 1 psi/ft or  
 331 0.226 bar/m (Cawley et al., 2005), and the hydrostatic gradient is assumed 0.54 psi/ft or 0.122  
 332 bar/m. Therefore, the pressure constraint is reduced to:

$$r_{p,W}^t \leq 1.66 \quad (6)$$

333

334 For the five wells of the system, at initial time and at top of Zone H just below the Charlie Shale, we  
 335 have  $p_{h,FA}^{t_0} = 248$  bar,  $p_{h,FB}^{t_0} = 245$  bar,  $p_{h,FC}^{t_0} = 236$  bar,  $p_{h,FD}^{t_0} = 245$  bar and  $p_{h,N}^{t_0} = 241$  bar.

336 To implement the migration constraint, we define a total target injection rate of  $Q_{inj}^{total}$  (million  
 337 tonnes per annum, hereafter denoted as  $MTY^{-1}$ ) to be apportioned between five injection wells  
 338 based on a time varying weight of injectivity index of each well with respect to sum of all wells'  
 339 injectivity indices, so that:

$$Q_{inj,W}^t = \begin{cases} f^{t-1} \times \left( \frac{Q_{inj}^{total} \times (\sum_{c=1}^{N_c} II_{W,c}^{t-1})}{\sum_{W \in \mathbb{W}1} (\sum_{c=1}^{N_c} II_{W,c}^{t-1})} \right) + (1 - f^{t-1}) \times \left( \frac{Q_{inj}^{total} \times (\sum_{c=1}^{N_c} II_{W,c}^{t-1})}{\sum_{W \in \mathbb{W}2} (\sum_{c=1}^{N_c} II_{W,c}^{t-1})} \right), & W \in \mathbb{W}2 \\ f^{t-1} \times \left( \frac{Q_{inj}^{total} \times (\sum_{c=1}^{N_c} II_{W,c}^{t-1})}{\sum_{W \in \mathbb{W}1} (\sum_{c=1}^{N_c} II_{W,c}^{t-1})} \right), & W = FC \end{cases} \quad (7)$$

340

341

$$f^{t-1} = \begin{cases} 1, & (x_{m,3}^{t-1} \times m_{CO_2}^{t-1}) \leq 0.1 \text{ million tonne} \\ 0, & (x_{m,3}^{t-1} \times m_{CO_2}^{t-1}) > 0.1 \text{ million tonne} \end{cases} \quad (8)$$

342

343 where:

- 344 ▪  $Q_{inj,W}^t$  is the "target" injection rate of well  $W$  at time  $t$ , actual injection rate can be lower
- 345 when the bottomhole pressure constraint for the well of interest is violated,
- 346 ▪  $II_{W,c}^{t-1}$  is the injectivity index of well  $W$  at connection (perforation)  $c$  and at time  $t - 1$ ,
- 347 calculated as  $II_{W,c}^{t-1} = Q_{inj,W}^{t-1} / (p_{bh,W,c}^{t-1} - P_e^{t-1})$ , where  $p_{bh,W,c}^{t-1}$  is the bottomhole pressure of
- 348 well  $W$ , at depth of connection  $c$  and at time  $t - 1$ , and  $P_e^{t-1}$  is the pressure at the vicinity
- 349 of connection  $c$  of well  $W$  at time  $t - 1$ ,
- 350 ▪  $N_W$  and  $N_c$  are the number of wells and number of connections for each well,
- 351 ▪  $\mathbb{W}1$  is a set of wells including all five injection wells,
- 352 ▪  $\mathbb{W}2$  is a set of all wells except for FC,
- 353 ▪  $f^{t-1}$  is a multiplier that is 1 when the amount of gaseous  $CO_2$  in Region 3 has not exceeded
- 354 the threshold of 0.1 million tonne. As soon as this threshold is exceeded,  $f^{t-1}$  is set to zero
- 355 ▪  $x_{m,3}^{t-1}$  and  $m_{CO_2}^{t-1}$  are as defined previously, the fraction of gaseous  $CO_2$  in Region 3 and the
- 356 total amount of  $CO_2$  (in moles) of gaseous and aqueous  $CO_2$  in all regions at time  $t - 1$ .

357 Above formulation apportions, initially, the total amount of available injection gas, to all five wells  
 358 proportional to their injectivity indices by the vector of  
 359  $Q_{inj}^{total} \times (\sum_{c=1}^{N_c} II_{W,c}^{t-1}) / (\sum_{W \in \mathbb{W}1} (\sum_{c=1}^{N_c} II_{W,c}^{t-1}))$ . However, since well FC contributes significantly to  
 360 the migration of  $CO_2$  outside the domes through Region 3 (the risk-prone region), this well is shut off  
 361 when the migration constraint is violated ( $f^{t-1} = 0$ ) and the total amount of gas is divided between  
 362 other wells by the vector of  $Q_{inj}^{total} \times (\sum_{c=1}^{N_c} II_{W,c}^{t-1}) / (\sum_{W \in \mathbb{W}2} (\sum_{c=1}^{N_c} II_{W,c}^{t-1}))$ . This approach ensures  
 363 maximum injection of  $CO_2$  into the two dome structures with the specific pressure and migration  
 364 constraints honoured.

365 The question in this work can be summarised as:

366 What is the maximum amount of  $CO_2$  that we can inject (actual cumulative injection denoted by  
 367  $q_{inj}^{cumul}$ ) into the two structures by five available injection wells so that:

- 368 ▪ the pressure constraint is not violated at any time;

369       ▪ a specific threshold of 0.1 million tonne of gaseous CO<sub>2</sub> is the maximum permissible amount  
370       that can migrate into the Zones J and K outside the dome structures (Region 3) of the model.

371 A range of  $Q_{inj}^{total}$  is prescribed in a 30-year injection period. The simulations are continued for a 50-  
372 year post injection monitoring period to record KPIs. The simulations are conducted on a HP ProLiant  
373 Server with 12-core processor, allowing parallel simulations at the time with Schlumberger's ECLIPSE  
374 E300 compositional simulator with CO2STORE option for CO<sub>2</sub> storage in saline aquifers. Each  
375 simulation takes about 17,849 seconds on the server.

376

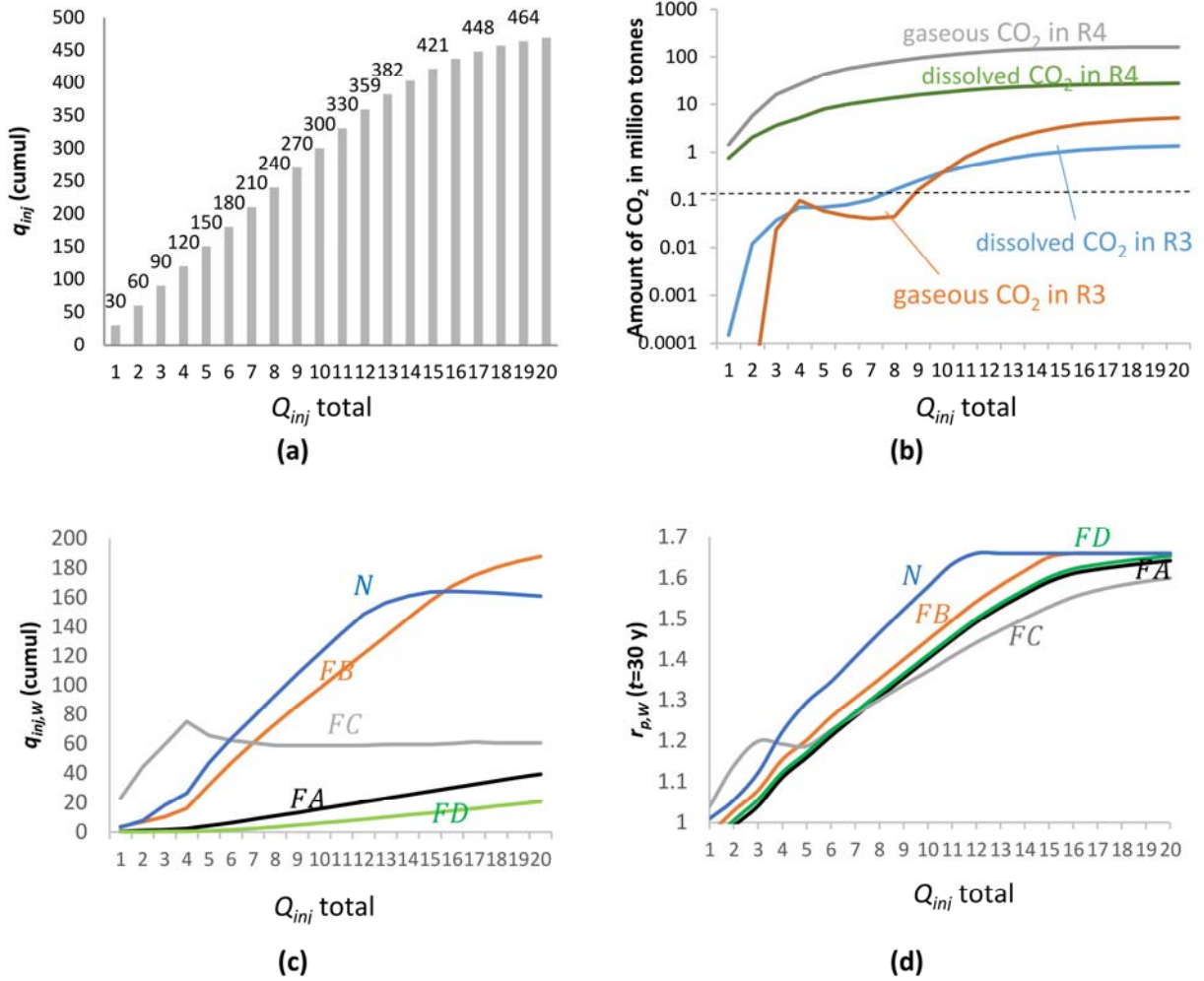
## 377       5. Results

378 In order to find the pressure and migration constrained injection strategy, we conduct 20  
379 simulations of  $Q_{inj}^{total}$  ranging from 1 to 20 MTY<sup>-1</sup>. The actual total injected CO<sub>2</sub> ( $q_{inj}^{cumul}$ ) is shown in  
380 Figure 5(a) for increasing  $Q_{inj}^{total}$ . It is observed that when  $Q_{inj}^{total} = 12$  MTY<sup>-1</sup>, the pressure constraint  
381 has led to  $q_{inj}^{cumul} < (30 \text{ years} \times Q_{inj}^{total})$ , thereby actual injected gas is less than the target injection.  
382 Figure 5(b) shows the maximum amount of spilled gaseous and dissolved CO<sub>2</sub> in Region 3 and 4 or  
383  $x_{m,R}^{t=30 \text{ years}} \times m_{CO_2}^{t=30 \text{ years}}$  in million tonnes. For this figure,  $Q_{inj}^{total} = 8$  MTY<sup>-1</sup> is a threshold injection  
384 rate above which the specifically defined threshold of 0.1 million tonnes CO<sub>2</sub> in Region 3 is violated.  
385 This is despite the fact that the injection strategy switches off the injection at FC to prevent the  
386 migration constraint being violated. In other words FA, FB and FD (only FB as will be shown later) are  
387 contributing to the migration for  $Q_{inj}^{total} > 8$  MTY<sup>-1</sup>. In Figure 5(b), we also showed the dissolved CO<sub>2</sub>  
388 versus  $Q_{inj}^{total}$  for Region 3 and Region 4 by end of the injection period.

389 Figure 5(c) shows the total actual injected gas for each well per  $Q_{inj}^{total}$ . The injectivity-index-based  
390 apportioning of rate chooses FC as the most suitable injection location between all five wells, and  
391 after FC is shut early in the simulation (for  $Q_{inj}^{total} = 4$  MTY<sup>-1</sup> and higher), N becomes the most suitable  
392 location. Then at  $Q_{inj}^{total} = 12$  MTY<sup>-1</sup> and higher, N initially gets higher proportions of injection, but  
393 because  $Q_{inj}^{total}$  is high, N violates the pressure constraint (Figure 5d) and therefore its injection rate  
394 is reduced so that by  $Q_{inj}^{total} = 16$  MTY<sup>-1</sup>, FB becomes the well with the highest cumulative gas  
395 injection of the system, despite the fact that FB itself reaches to the threshold of  $r_{p,W}^t = 1.66$   
396 sometime in the simulation. For all the simulations,  $r_{p,W}^t$  at 30 years for each well and for each  
397  $Q_{inj}^{total}$  is shown in Figure 5(d).

398 In our 3D model, FA and FD have relatively low injectivity indices and therefore they are not  
399 favourable for injection. The low injectivity is also manifested for high  $Q_{inj}^{total}$  where even small  
400 proportions of injection gas lead to FA and FD reaching  $r_{p,W}^t = 1.66$  during the simulation (Figure  
401 5d). A favourable location of FC (next to the Forties spill point to Zones J and K), and then FB which is  
402 located away from the spill point to Zones J and K and away from abrupt discontinuity of Zones J and  
403 K towards the east outweigh the injectivity of FA and FD.

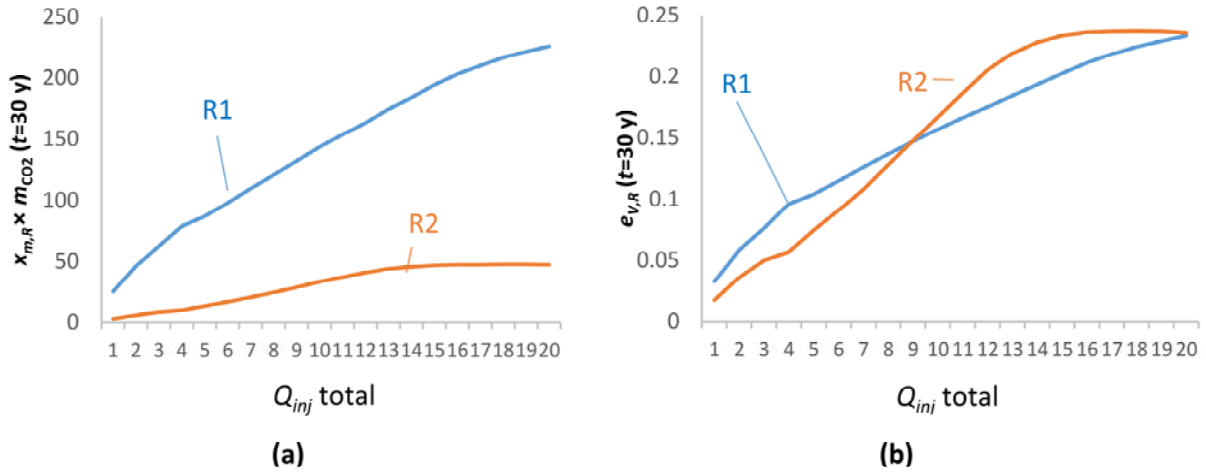
404



405

406 **Figure 5.** (a) Cumulative (actual) gas injected versus  $Q_{inj}^{total}$ , (b) the amount of CO<sub>2</sub> in gaseous phase in Region 3  
 407 versus  $Q_{inj}^{total}$ , (c) Cumulative (actual) gas injected for each well versus  $Q_{inj}^{total}$ , and (d) the ratio of  
 408 pressure increase at year 30 for each well versus  $Q_{inj}^{total}$ .

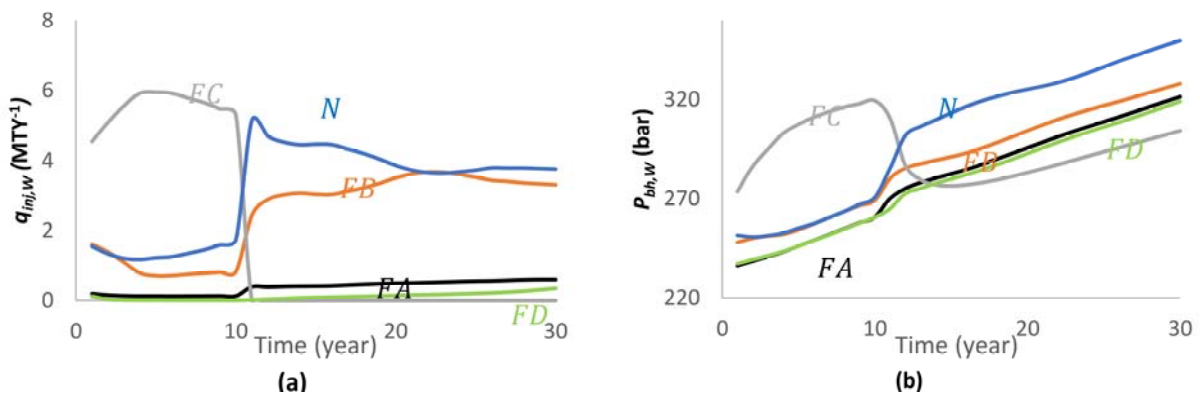
409 Figure 6 shows the profiles of gaseous CO<sub>2</sub> ( $x_{m,R}^{t=30 \text{ years}} \times m_{CO_2}^{t=30 \text{ years}}$ ) and fraction of capacity  
 410 utilised by increase in  $Q_{inj}^{total}$ . For Nelson we reach plateaus for both quantities at  $Q_{inj}^{total} = 14 \text{ MTY}^{-1}$ .  
 411 Therefore increase in  $Q_{inj}^{total}$  does not necessarily lead to increase in fraction of capacity utilised.  
 412 Figure 6(a) shows that Forties dome is capable of accommodating around 121 million tonnes of CO<sub>2</sub>  
 413 applying the selected injection rate of  $Q_{inj}^{total} = 8 \text{ MTY}^{-1}$  (corresponding to a total amount of injection  
 414 of 240 million tonnes). For Nelson the value is 24 million tonnes. Therefore, based on our migration  
 415 constraint of less than 0.1 million tonnes of gaseous CO<sub>2</sub> in Region 3 (the pressure constraint is not  
 416 limiting injection for  $Q_{inj}^{total} = 8 \text{ MTY}^{-1}$ ), the dynamic capacities of Forties and Nelson stand at 121  
 417 million tonnes and 24 million tonnes respectively. Corresponding fraction of capacity utilised for  
 418 Forties and Nelson are shown in Figure 6(b), where at  $Q_{inj}^{total} = 8 \text{ MTY}^{-1}$ , both  $e_{V,R1}^{t=30 \text{ years}}$  and  
 419  $e_{V,R2}^{t=30 \text{ years}}$  curves intersect each other at 0.147.



420

421 **Figure 6.** (a) The amount of CO<sub>2</sub> in gaseous phase at Regions 1 and 2 versus  $Q_{inj}^{total}$ , and (b) the volumetric  
 422 storage efficiency for Regions 1 and 2 (Forties and Nelson dome structures, respectively) at year 30  
 423 versus  $Q_{inj}^{total}$ .

424 To visualise the distribution of CO<sub>2</sub> in the 3D model, for monitoring purposes we additionally  
 425 simulate a 200 year post-injection period using  $Q_{inj}^{total} = 8 \text{ MTY}^{-1}$  and its corresponding injection  
 426 strategy with the well injection rates shown in Figure 7(a) and resultant bottomhole pressure  
 427 profiles in Figure 7(b) for the 30-year injection period.

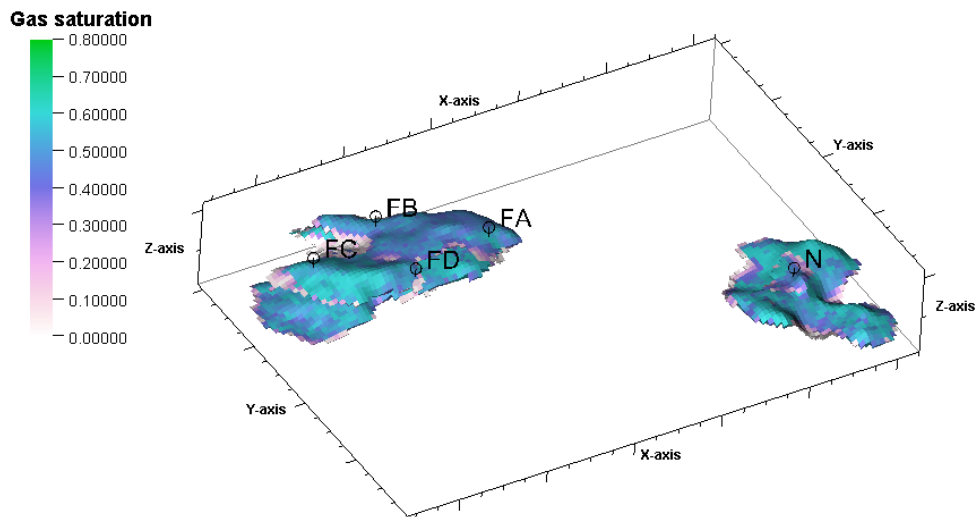


428

429 **Figure 7.** (a) The dynamically varying injection rates for the five injection wells corresponding to  $Q_{inj}^{total} = 8 \text{ MTY}^{-1}$   
 430 <sup>1</sup> for the 30-year injection period. FC is shut for year 10 because of the migration constraint. (b)  
 431  $P_{bh,W}^t$  for the five injection wells corresponding to  $Q_{inj}^{total} = 8 \text{ MTY}^{-1}$  for the 30-year injection period.  
 432 None of the wells are affected by the pressure constraint at this  $Q_{inj}^{total}$

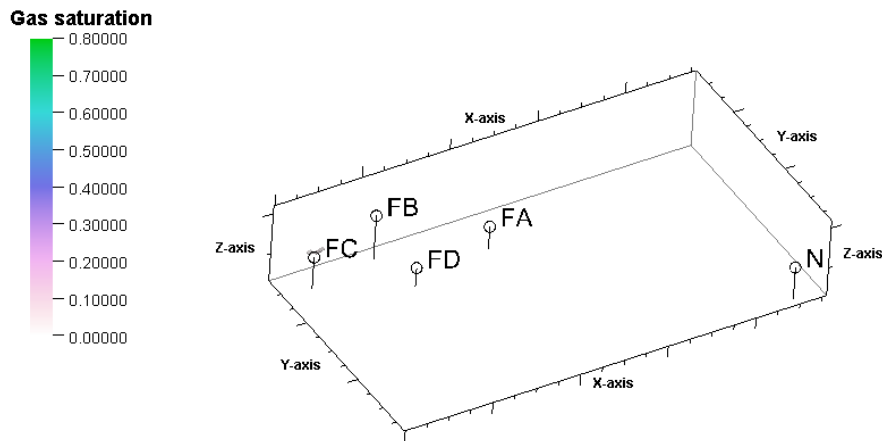
433 Figure 8(a) shows the spread of CO<sub>2</sub> gas saturation after 230 years of simulation for all regions of the  
 434 3D model. We filtered out the blocks that have less than 0.01 gas saturation. Figure 8(b) shows the  
 435 extent of gaseous CO<sub>2</sub> ( $S_g > 0.01$ ) outside the dome structures in Region 3 only. Clearly there is only a  
 436 negligible amount of gas in Region 3. Figure 8(c) shows the extent of gaseous CO<sub>2</sub> ( $S_g > 0.01$ ) outside  
 437 the dome structures in Region 4 only. Underneath the Nelson dome, a significant amount of gas has  
 438 been stored, because the Nelson well, N, has been on operation with a high injection rate after well  
 439 FC is shut.





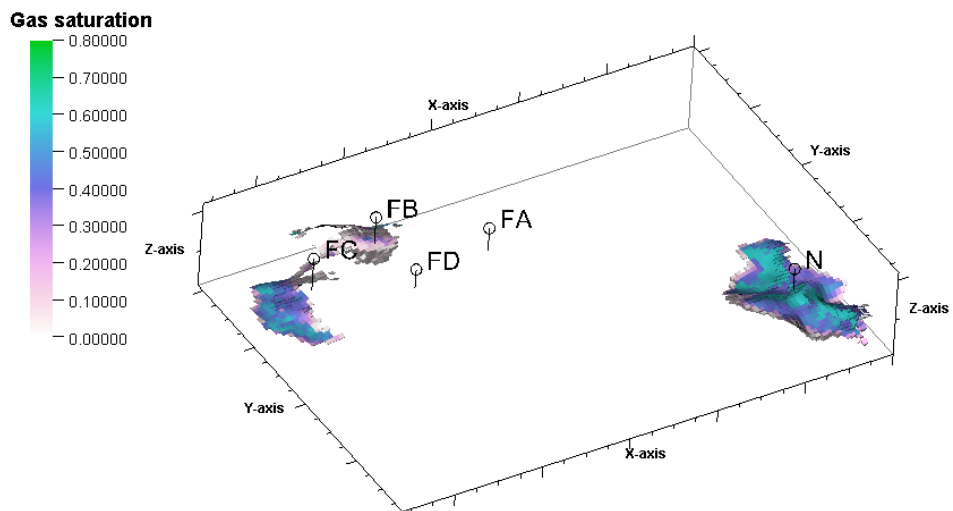
440  
441

(a)



442  
443

(b)



444  
445

(c)

446 **Figure 8.** The gas saturation ( $S_g$ ) distribution 200 years after  $\text{CO}_2$  injection stopped. (a) The distribution for all  
447 blocks with  $S_g > 0.01$ , (b) the distribution for blocks belonging to Region 3 only with  $S_g > 0.01$ , and (c)  
448 the distribution for blocks belonging to Region 4 only with  $S_g > 0.01$ .

## 6. Conclusions and future work

449 The authors have constructed a detailed geological model that encompasses the Forties and Nelson  
450 dome structures and the surrounding aquifer system located in the UK Central North Sea. Historical  
451 data for hydrocarbon production was used to calibrate the model in terms of the aquifer support for  
452 pressure by scaling the pore volumes at the boundaries of the model. A number of key performance  
453 indicators for CO<sub>2</sub> storage including the ratio of pressure increase, regional mass fractions, and  
454 fraction of capacity utilised alongside the injection strategy constrained by both pressure and  
455 migration were defined. It was assumed that the structures are fully saturated with brine and  
456 consequently our simulations are based on CO<sub>2</sub> storage in saline aquifers.  
457

458 The injection simulation results for a range of input total injection target rates were used to extract  
459 the dynamically varying injection rates weighted by the injectivity indices of the wells. The injection  
460 scenarios also honoured the pressure and migration constraints for five wells belonging to the five  
461 platforms of the two structures. It was shown that, based on the specific threshold of well  
462 bottomhole pressures to stay below 1.66 times the initial hydrostatic pressure, and the migration  
463 constraint of having less than 0.1 million tonnes of gaseous CO<sub>2</sub> in Zones J and K outside the dome  
464 structures, 121 and 24 million tonnes of CO<sub>2</sub> can be stored in the Forties and Nelson dome  
465 structures, respectively. This was achieved by injecting 8 million tonnes of CO<sub>2</sub> per year into the two  
466 structures for 30 years. According to the simulation results, 80 million tonnes of CO<sub>2</sub> from the total  
467 240 million tonnes is also expected to migrate in gas phase outside the regions below the Charlie  
468 Shale (which we assume it bears less risk of leakage to the surface in comparison with the region  
469 above field-wide Charlie Shale).

470 The calculated total capacity of 145 MT CO<sub>2</sub> corresponds to a total reservoir gas volume of 225  
471 million m<sup>3</sup> combined from both structures extracted from the simulator outputs<sup>†</sup>. Considering that  
472 the original pore volume of the whole domain before application of PVM is 8,552 million m<sup>3</sup>, the  
473 storage efficiency is 0.026 or 2.6%. This value agrees with the range of regional-scale storage  
474 efficiency values calculated to be 2% by Obi and Blunt, (2006), 2.3% by (Smith *et al.* 2011) and 3.5%  
475 by Goater *et al.* (2013) for UK Forties formation, and assumed to be 2% for Dutch CO<sub>2</sub> storage  
476 candidate sites by Wildenborg *et al.*, (1998), Damen *et al.*, (2009), and Ramírez *et al.* (2010) and in  
477 the range of 0.2% - 2% by SCCS (2009) for the UK North Sea formations. We conclude that in our  
478 study a combination of detailed geological data assimilation, dome stratigraphical volume  
479 calculation (using the zones' horizons and water-oil contact), and constraining the simulations by  
480 pressure and migration, have resulted in reliable storage capacity estimates for Forties and Nelson  
481 dome structures.

482 Future work includes:

- 483     ▪ Considering a three phase CO<sub>2</sub>-oil-brine system that accounts for oil remaining unproduced  
484     from the hydrocarbon production stage. In this way, the feasibility and potentials of CO<sub>2</sub>-  
485     EOR (Enhanced Oil Recovery) can be assessed and consequently a more realistic situation in  
486     which the reservoirs are not assumed fully depleted can be considered.
- 487     ▪ Accounting for the uncertainties in the petrophysical properties of the geological model.

---

<sup>†</sup> This value can also be obtained by assuming a reservoir condition density of CO<sub>2</sub>=600 kg.m<sup>-3</sup>, 145 million tonnes / 600 kg.m<sup>-3</sup> = 241 million m<sup>3</sup>

## 488 **Acknowledgements**

489 The authors appreciate the constructive comments of the anonymous reviewers of the paper. This  
490 research was carried out as part of the UK Research Councils' Energy Programme funded consortium  
491 projects "Multiscale Whole Systems Modelling and Analysis for CO<sub>2</sub> Capture, Transport and Storage",  
492 Grant Reference: NE/H01392X/1 and "CO<sub>2</sub> Injection and Storage - Short and Long-term Behaviour at  
493 Different Spatial Scales", Grant Reference: EP/K035967/1. The computational resources were  
494 provided by the University of Manchester EPS funding. The authors would like to thank this  
495 institution.

496

## 497 **Appendix – Area-Type definition for *Forties Sandstone Member***

498 The Forties Sandstone Member comprises submarine fan sandstones made up of a huge number of  
499 interconnected amalgamated channels and interchannel areas that change laterally and vertically  
500 creating a very complex 'plumbing system'. The 'Forties Fan' can be regarded as an open system -  
501 though it is probably closed on its south-eastern, south western and north-eastern sides. It is  
502 probably open to the northwest.

503 The Forties fan is 300 km by 100 km at its widest spread and trends NW-SE and, in general, to the SE  
504 the reservoirs will become deeper, and thinner, will have lower mean NTG and lower, but still fair to  
505 good, porosities, will have poorer permeabilities (by factor of 10 less). In addition, to the SE, any  
506 structural closures present are more likely to be formed by salt movement.

507 Numerous hydrocarbon fields are located in different parts of the Forties fan:

- 508     ▪ **Proximal:** mostly channelised turbidite reservoirs such as Forties and Nelson fields, high NTG  
509       (65%), porosity 23-26%, permeabilities hundreds of mD
- 510     ▪ **Distal:** turbidite reservoirs less frequently channelised such as Pierce and Starling fields, more  
511       typically overlapping lobes and/or sheets, lower NTG (50%), porosity 16-23%, permeabilities  
512       tens of mD

513 There is a clear and progressive downdip thinning: 259 m at the Forties Field (proximal area) and 137  
514 m at the Pierce Field (distal area). Three potential *Area Types* have been identified based primarily  
515 on palaeogeography (*i.e.*, location on fan complex) (Figure 1 in the manuscript).

### 516 **Area Type 1**

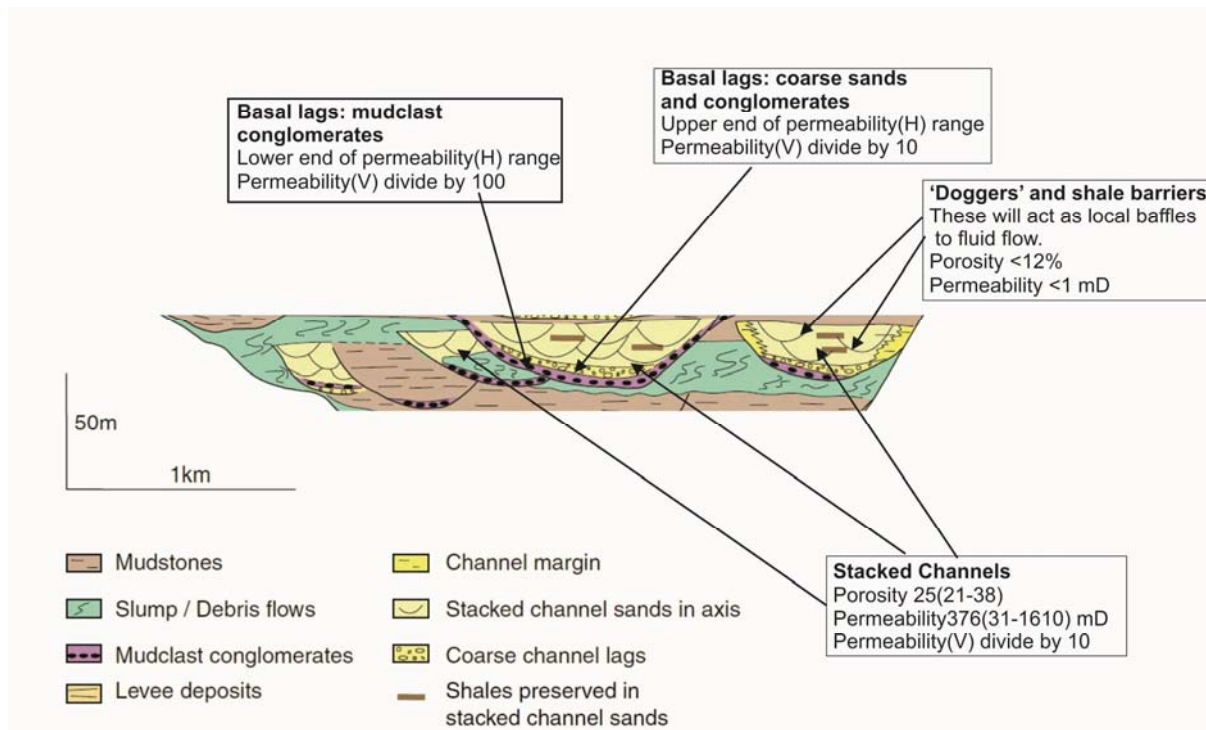
517 The 3D model has been built from an area that includes the Forties and Nelson fields located in the  
518 central part of the Forties fan. The reservoir in this 3D model exhibits lateral and vertical variation in  
519 petrophysical parameters, reflecting the evolution of the Forties submarine fan in a relatively  
520 proximal location. The model has been attributed using data from the Forties and Nelson oil fields  
521 and information from wells drilled in the area. Each zone in the model is divided into two facies  
522 associations namely 'channel' and 'interchannel' areas:

#### 523 ***Amalgamated channels***

524 There are four elements to the amalgamated channels – channel sands, low permeability basal lags,  
525 high permeability basal lags and intra channel doggers as shown in Figure A1.

526 **Interchannel areas**

527 The 'Interchannel' areas and associated channel margins contain muddy debris flows, slump  
 528 deposits, thin-bedded turbidites and mudstones. Mudstones form vertical permeability barriers to  
 529 the sandstones present.



530  
 531 **Figure A1.** Illustration of different facies in Area Type 1. Cartoon modified after Mayall et al. (2006)

532 Table 2 in manuscript reports the facies-dependent attributes of the Area Type 1 geological model,  
 533 and Babaei *et al.* (2016, Tables 1 and 2) summarises the objects' shapes and geometrical parameters  
 534 used for representing the different facies in Area Type 1.

535 **Area Type 2**

536 Area Type 2 reservoir attribution is based on data from Montrose, Arbroath, Arkwright and South  
 537 Everest fields and core measurements from two wells. The following table reports the data for Area  
 538 Type 2.

539 **Table A1 – Data for Area Type 2**

Data source	Depth to top	Thickness	Porosity	Permeability	NTG
Arbroath & Montrose fields (Crawford et al., 1991; Hogg 2003)	2447.5 & 2451 m	100.6(79.2 – 134.1)	24(3-30)	80(1-2000) Commonly 70 to 90 mD	0.5(0.3 – 0.8)
Arkwright (Kantorowicz 1999)	2578 m	153 m	19.25(15.9 – 21.0)	38.4(24-78)	0.78(0.61 – 0.91)
South Everest (Thompson & Butcher 1991)	2591		21	46	0.67

<i>Well 22/18- 5</i>			22.5(1.5-29)	53.8(0.001-177)	
<i>Well 22/23a- 3</i>			20.44(2.4-28.6)	78.8(0.01-202) Reservoir sands 39(0.01-202) All values	
<i>SUMMARY</i>	2517 m		22(16-30)	80(1-1250)	0.61(0.3-0.91)

540 **Area Type 3**

541 Structures and closures are compact, generally circular, and smaller. The structures are often due to  
542 underlying salt movement. Radial faults may act as baffles but unlikely to compartmentalise  
543 reservoirs (Birch and Haynes, 2003; Kantorowicz et al., 1999). The following table reports the data  
544 for Area Type 3.

545

546 **Table A2 – Data for Area Type 3**

<b>Data source</b>	<b>Depth to top</b>	<b>Thickness</b>	<b>Porosity</b>	<b>Permeability</b>	<b>NTG</b>
<i>Pierce</i>		145.8 m	18(16-20)	19(1-40)	0.47(0.01-0.77)
<i>Mungo</i>		100 – 400 m	19 -24	10-50	0.43-0.63 to 0.25
<i>Machar</i>			21 average	5-50	
<i>North Everest (Thompson &amp; Butcher 1991)</i>	2560		19	16	0.55
<i>Well 23/22a- 3</i>			17(2.2-22.5)	11.5(0.01-70)	
<i>Well 29/03a- 7</i>		141.7 m	22(2.3-27.1)	297(0.004-675)	
<i>SUMMARY</i>			20(16-27)	20(1-600)	0.51(0.01-0.77)

547

## 548 References

- 549 Babaei, M., I. Pan, A. Korre, J.-Q. Shi, R. Govindan, S. Durucan and M. Quinn (2016), CO<sub>2</sub> storage well  
550 rate optimisation in the Forties sandstone of the Forties and Nelson reservoirs using evolutionary  
551 algorithms and upscaled geological models, *International Journal of Greenhouse Gas Control* 50,  
552 1–13.
- 553 Bachu, S. (2015), Review of CO<sub>2</sub> storage efficiency in deep saline aquifers, *International Journal of*  
554 *Greenhouse Gas Control* 40, 188–202.
- 555 Birch, P., and J. Haynes (2003), The Pierce Field, Blocks 23/22a, 23/27, UK North Sea. In: Gluyas, J.G.  
556 & Hitchens, H.M. (eds). United Kingdom Oil and Gas Fields, Commemorative Millennium Volume.  
557 Geological Society, London, Memoir, 20, pp. 647-659.
- 558 Birkholzer, J.T., C.M. Oldenberg, and Q. Zhou (2015), CO<sub>2</sub> migration and pressure evolution in deep  
559 saline aquifers, *International Journal of Greenhouse Gas Control* 40, 203–220.
- 560 Brand, P., P. Clyne, F. Kirkwood, and P. Williams (1996), The Forties Field-20 Years Young, *Journal of*  
561 *Petroleum Technology*, 48(4), 280–291.
- 562 Burton, M.M., N. Kumar, S.L. and Bryant (2008), Time-dependent injectivity during CO<sub>2</sub> storage in  
563 aquifers, in the 2008 SPE/DOE Improved Oil Recovery Symposium held in Tulsa, Oklahoma, U.S.A.,  
564 19–23 April 2008.
- 565 Cawley, S.J., M.R. Saunders, Y. Le Gallo, B. Carpentier, S. Holloway, G.A. Kirby, T. Bennison, L.  
566 Wickens, and R. Wikramaratna, T. Bidstrup, S.L.B. Arkley and M.A.E. Browne, and J.M. Ketzer  
567 (2005), *The NGCAS Project-Assessing the potential for EOR and CO<sub>2</sub> storage at the Forties Oil field,*  
568 *Offshore UK-Results from the CO<sub>2</sub> Capture Project, v. 2: Geologic Storage of Carbon Dioxide with*  
569 *Monitoring and Verification*, SM Benson, Elsevier Science, London.
- 570 Crawford, R., R.W. Littlefair, and L.G. Affleck (1991), The Arbroath and Montrose Fields, Blocks  
571 22/17, 18, UK North Sea. In: Abbotts, I.L. (ed). United Kingdom Oil and Gas Fields, 25 Years  
572 Commemorative Volume. Geological Society Memoir No. 14, pp. 211-217.
- 573 Damen, K., A. Faaij, W. Turkenburg (2009), Pathways towards large-scale implementation of CO<sub>2</sub>  
574 capture and storage: A case study for the Netherlands, *International Journal of Greenhouse Gas*  
575 *Control*, 3(2), pp 217-236
- 576 DECC (2007), Well Production Data, Department for Business, Enterprise and Regulatory Reform,  
577 [online] Available from: <https://www.og.decc.gov.uk/information/wells/pprs/welldataindex.htm>
- 578 DECC (2013), UK Monthly Oil Production Data, Department of Energy and Climate Change, [online]  
579 Available from: [https://www.og.decc.gov.uk/pprs/full\\_production.htm](https://www.og.decc.gov.uk/pprs/full_production.htm)
- 580 Doughty, C. and K. Pruess (2004), Modeling Supercritical Carbon Dioxide Injection in Heterogeneous  
581 Porous Media, *Vadose Zone Journal* 3 (3). Soil Science Society: 837–47.
- 582 Ennis-King, J. and L. Paterson (2005), Role of Convective Mixing in the Long-Term Storage of Carbon  
583 Dioxide in Deep Saline Formations, *SPE Journal* 10 (3), Society of Petroleum Engineers: 349–56.
- 584 Espie, A. (2001), Options for establishing a North Sea geological storage hub, in *Greenhouse Gas*  
585 *Control Technologies: Proceedings of the Fifth International Conference on Greenhouse Gas*  
586 *Control Technologies*, CSIRO Publishing, Collingwood, Victoria, Australia, pp. 266–271.
- 587 Flett, M., R. Gurton, and G. Weir (2007), Heterogeneous Saline Formations for Carbon Dioxide  
588 Disposal: Impact of Varying Heterogeneity on Containment and Trapping, *Journal of Petroleum*  
589 *Science and Engineering* 57 (1). Elsevier: 106–18.
- 590 Frailey, S. M. (2009), Methods for Estimating CO<sub>2</sub> Storage in Saline Reservoirs, *Energy Procedia* 1 (1).  
591 Elsevier: 2769–76.
- 592 Goater, A.L., B. Bijeljic and M.J. Blunt (2013), Dipping open aquifers—The effect of top-surface  
593 topography and heterogeneity on CO<sub>2</sub> storage efficiency, *International Journal of Greenhouse*  
594 *Gas*, 17, pp. 318-331.
- 595 Hempton, M., J. Marshall, S. Sadler, N. Hogg, R. Charles, and C. Harvey (2005), Turbidite reservoirs of  
596 the Sele Formation, Central North Sea: geological challenges for improving production, in  
597 *Geological Society, London, Petroleum Geology Conference series*, vol. 6, pp. 449–459.

598 Hogg, A.J.C. (2003), The Montrose, Arbroath and Arkwright Fields, Blocks 22/17, 22/18, 22/23a, UK  
599 North Sea. In: Gluyas, J.G. & Hitchens, H.M. (eds). United Kingdom Oil and Gas Fields,  
600 Commemorative Millennium Volume. Geological Society, London, Memoir, 20, pp. 611-616.

601 Holt, T., J.-I. Jensen, and E. Lindeberg (1995), Underground storage of CO<sub>2</sub> in aquifers and oil  
602 reservoirs, *Energy Conversion and Management*, 36(6), 535–538.

603 Hughes, D., D. Teeuw, C. Cottrell, and J. Tollas (1990), Appraisal of the Use of Polymer Injection To  
604 Suppress Aquifer Influx and To Improve Volumetric Sweep in a Viscous Oil Reservoir, *SPE*  
605 *Reservoir Engineering*, 5(1), 33–40.

606 IPCC (2005) Intergovernmental Panel on Climate Change: Special Report on Carbon Dioxide Capture  
607 and Storage, (ed.) Metz, B. and Davidson, O. and de Cornick, H. and Loos, M. and Meyer, L.,  
608 Prepared by Working Group III of the Intergovernmental Panel on Climate Change Published for  
609 the Intergovernmental Panel on Climate Change

610 Kantorowicz, J. D., I.J. Andrews, S. Dhanani, M. Gillis, C. Jennings, P.J. Lumsden, G. Orr, R.W. Simm,  
611 and J. Williams (1999), Innovation and risk management in a small subsea-tieback: Arkwright  
612 Field, Central North Sea, UK. In: Fleet, A. J. & Boldy, S. A. R. (eds) Petroleum Geology of Northwest  
613 Europe: Proceedings of the 5th Conference, 1125-1134. Petroleum Geology '86 Ltd. Published by  
614 the Geological Society, London.

615 Ketzer, J.M., B. Carpentier, Y. Le Gallo, and P. Le Thiez (2005), Geological sequestration of CO<sub>2</sub> in  
616 mature hydrocarbon fields. Basin and reservoir numerical modelling of the Forties Field, North  
617 Sea, *Oil & gas science and technology*, 60(2), 259–273.

618 Kulpecz, A. A., and L. C. van Geuns (1990), Geological Modeling of a Turbidite Reservoir, Forties Field,  
619 North Sea, in *Sandstone Petroleum Reservoirs*, edited by Barwis, John H. and McPherson, John G.  
620 and Studlick, Joseph R.J., pp. 489–507, Springer New York.

621 Kumar, A., M. Noh, G.A. Pope, K. Sepehrnoori, S. Bryant, and L.W. Lake (2004), Reservoir Simulation  
622 of CO<sub>2</sub> Storage in Deep Saline Aquifers. In *SPE/DOE Symposium on Improved Oil Recovery*.

623 Kunka, J., G. Williams, B. Cullen, J. Boyd-Gorst, G. Dyer, J. Garnham, A. Warnock, J. Wardell, A. Davis,  
624 and P. Lynes (2003), The Nelson Field, Blocks 22/11, 22/61, 22/7, 22/12a, UK North Sea,  
625 *Geological Society, London, Memoirs*, 20(1), 617–646.

626 Liao, C., X. Liao, X. Zhao, H. Ding, X. Liu, Y. Liu, J. Chen, and N. Lu (2014), Comparison of Different  
627 Methods for Determining Key Parameters Affecting CO<sub>2</sub> Storage Capacity in Oil Reservoirs .  
628 *International Journal of Greenhouse Gas Control* 28 (0): 25 – 34.

629 Mathias, S. A., P. E. Hardisty, M. R. Trudell, and R. W. Zimmerman (2009), Approximate Solutions for  
630 Pressure Buildup during CO<sub>2</sub> Injection in Brine Aquifers. *Transport in Porous Media* 79 (2).  
631 Springer: 265–84.

632 Mayall, M., E. Jones, and M. Casey (2006). Turbidite channel reservoirs – Key elements in facies  
633 prediction and effective development. *Marine and Petroleum Geology*, Vol. 23, pp.821-841.

634 van der Meer, L.G.H. (1995), The CO<sub>2</sub> Storage Efficiency of Aquifers. *Energy Conversion and*  
635 *Management* 36 (6). Elsevier: 513–18.

636 van der Meer, L.G.H., and P.J.P. Egberts (2008), A general method for calculating subsurface storage  
637 capacity, OTC Paper 19309.

638 van der Meer, L.G.H. and F. Yavuz (2009), CO<sub>2</sub> storage capacity calculations for the Dutch subsurface,  
639 *Energy Procedia* 1: 2615–2622.

640 Obi, E. O. I., and M.J. Blunt (2006), Streamline-based simulation of carbon dioxide storage in a North  
641 Sea aquifer, *Water Resources Research*, 42(3).

642 Ozah, R.C., S. Lakshminarasimhan, G.A. Pope, K. Sepehrnoori, and S. L. Bryant (2005), Numerical  
643 Simulation of the Storage of Pure CO<sub>2</sub> and CO<sub>2</sub>-H<sub>2</sub>S Gas Mixtures in Deep Saline Aquifers. In *SPE*  
644 *Annual Technical Conference and Exhibition*.

645 Ramírez, A., S. Hagedoorn, L. Kramers, T. Wildenborg, and C. Hendriks (2010), Screening CO<sub>2</sub> storage  
646 options in The Netherlands, *International Journal of Greenhouse Gas Control*, 4(2).

647 Robertson, J., N.R. Goult, and R.E. Swarbrick (2013), Overpressure distributions in Palaeogene  
648 reservoirs of the UK Central North Sea and implications for lateral and vertical fluid flow,  
649 *Petroleum Geoscience*, 19, Geological Society of London, pp. 223-236.

650 SCCS (2009), Opportunities for CO<sub>2</sub> Storage around Scotland — an integrated strategic research  
651 study, [online] Available from: [http://carbcap.geos.ed.ac.uk/website/publications/regionalstudy/](http://carbcap.geos.ed.ac.uk/website/publications/regionalstudy/CO2-JointStudy-Full.pdf)  
652 [CO<sub>2</sub>-JointStudy-Full.pdf](http://carbcap.geos.ed.ac.uk/website/publications/regionalstudy/CO2-JointStudy-Full.pdf)

653 Simpson, A., and R. Paige (1991), Advances in Forties field water injection, *Offshore Europe*.

654 Smith, D.J., D.J. Noy, S. Holloway and R.A. Chadwick (2011), The impact of boundary conditions on  
655 CO<sub>2</sub> storage capacity estimation in aquifers, *Energy Procedia*— pp. 4828-4834.

656 Stevens, S. H., V. A. Kuuskraa, and J. Gale (2000), Sequestration of CO<sub>2</sub> in depleted oil and gas fields:  
657 global capacity, costs and barriers, in *Proceedings of the 5th International Conference on*  
658 *Greenhouse Gas Control Technologies (GHGT-5)*, DJ Williams, RA Durie, P. McMullan, CAJ Paulson  
659 and AY Smith (eds.), pp. 13–16.

660 Thompson, P.J. and P.D. Butcher (1991), The geology and geophysics of the Everest Complex. In:  
661 Spencer, A.M. (ed). Generation, accumulation and production of Europe’s hydrocarbons. Special  
662 publication of the European Association of Petroleum Geoscientists No. 1, pp. 89-98. Oxford  
663 University Press, Oxford. The European Association of Petroleum Geoscientists.

664 Whyatt, M., J. Bowen, and D. Rhodes (1992), The Nelson Field: a successful application of a  
665 development geoseismic model in North Sea exploration, *Geological Society, London, Special*  
666 *Publications*, 67(1), 283–305.

667 Wildenborg, T., H. Dudok van Heel and F. Van Bergen (2003), CO<sub>2</sub> Storage Potential of Saline Aquifers  
668 in the Netherlands Onshore Region. Study Area A, Southern North Sea, Netherlands Institute of  
669 Applied Geoscience TNO – National Geological Survey, Utrecht.

670 Wills, J. (1991), The Forties Field, Block 21/10, 22/6a, UK North Sea, *Geological Society, London,*  
671 *Memoirs*, 14(1), 301–308.

672 Zhou, Q., J. T. Birkholzer, C.-F. Tsang, and J. Rutqvist (2008), A method for quick assessment of CO<sub>2</sub>  
673 storage capacity in closed and semi-closed saline formations, *International Journal of Greenhouse*  
674 *Gas Control*, 2(4), 626–639.

675 Yamamoto, H., K. Zhang, K. Karasaki, A. Marui, H. Uehara, and N. Nishikawa (2009), Numerical  
676 Investigation Concerning the Impact of CO<sub>2</sub> Geologic Storage on Regional Groundwater Flow.  
677 *International Journal of Greenhouse Gas Control* 3 (5). Elsevier: 586–99.

678